





Anisotropic Metasurface for Ultrafast Polarization Control via All-Optical Modulation

Giulia Crotti^{1,2}, Mert Akturk¹, Andrea Schirato^{1,2}, Vincent Vinel³, Remo Proietti Zaccaria^{2,4}^a,
Margherita Maiuri^{1,5}, Anton A. Trifonov⁷, Ivan C. Buchvarov^{7,8}, Dragomir N. Neshev⁹^b,
Giuseppe Leo³, Giulio Cerullo^{1,5}^c and Giuseppe Della Valle^{1,5,6}^d

¹*Department of Physics, Politecnico di Milano, 20133 Milano, Italy*

²*Istituto Italiano di Tecnologia, 16163, Genova, Italy*

³*Laboratoire Matériaux et Phénomènes Quantiques, MPQ UMR 7162, Université de Paris, CNRS, 75013, Paris, France*

⁴*Cixi Institute of Biomedical Engineering, Ningbo Institute of Industrial Technology,
Chinese Academy of Sciences, Ningbo 315201, China*

⁵*INFN, Consiglio Nazionale Delle Ricerche, 20133, Milano, Italy*

⁶*INFN, Sezione di Milano, I-20133 Milano, Italy*

⁷*John Atanasoff Center for Bio and Nano Photonics (JAC BNP), 1164 Sofia, Bulgaria*

⁸*Faculty of Physics, St. Kliment Ohridski University of Sofia, 5 James Bourchier Boulevard, 1164 Sofia, Bulgaria*

⁹*ARC Centre of Excellence for Transformative Meta-Optical Systems (TMOS), Research School of Physics,
Australian National University, Acton, ACT 2601, Australia*

Keywords: Ultrafast Photonics, All-Optical Polarization Control, Reconfigurable Metasurfaces.


Abstract: The ability to manipulate light polarization at an ultrafast speed is a challenging goal in the field of Photonics: sub-picosecond control of polarization is a fundamental functionality for a variety of applications, including the development of free-space optical links for robust information encoding. To this aim, an important paradigm consists in employing metasurfaces as platforms which can be reconfigurable by all-optical means, *i.e.* upon illumination by an energetic femtosecond laser pulse. Here, we present giant all-optical modulations of dichroism in an anisotropic AlGaAs metasurface. An optimized design allows to exploit a sharp extended resonance of the nanostructure in the desired spectral range, where the pump-induced band-filling effect is the dominant process presiding over the ultrafast change of permittivity.


1 INTRODUCTION


Polarization is one of the fundamental degrees of freedom of light. Ultrafast, active control of it is a crucial functionality for a plethora of applications in various fields, ranging from classic and quantum information manipulation and encoding (Stanciu et al., 2007; Flamini et al., 2018) to modulation of material processes, such as molecular orientation (Fleischer et al., 2011) and lattice excitation (Först et al., 2011), to probing polarization-sensitive chemical and biological systems (e.g. chiral molecules).


In order to develop reconfigurable devices, operating in the THz speed regime, the most promising approach consists in adopting all-optical schemes. In these, an energetic femtosecond laser pulse is employed to trigger a third-order optical nonlinearity, which provides modification of the material permittivity of the system, thus modulating the optical response on a sub-picosecond timescale.

Within this framework, some possible platforms have been identified for efficient polarization control. Polarization switching with an extinction rate of 91 and a switch-on time of 800 fs has been demonstrated in a perfect absorber consisting of an In-doped cadmium-oxide film with a gold capping (Yang et al., 2017); synthesis and switching of light polarization with up to 60° rotation of the polarization ellipse have been achieved in a nonlinear metamaterial based on

^a <https://orcid.org/0000-0002-4951-7161>

^b <https://orcid.org/0000-0002-4508-8646>

^c <https://orcid.org/0000-0002-9534-2702>

^d <https://orcid.org/0000-0003-0117-2683>

a gold nanorod array embedded in a Al_2O_3 matrix (Nicholls et al., 2017). Another possibility is represented by epsilon-near-zero materials-based devices, such as in (Wang et al., 2021), where indium titanium oxide is coupled to gold nanoantennas.

An alternative route is represented by metasurfaces, which are planar arrangements of tightly packed nanoresonators, and, as such, are both ultra-compact and highly tunable. Consequently, they constitute the ideal candidate for the development of integrated photonic devices. A relevant example of polarization control is illustrated in a paper by some of the present authors (Schirato et al., 2020), where a sizeable dichroic response is induced in an *isotropic* plasmonic metasurface via photo-induced excitation of out-of-equilibrium carriers with a non-uniform spatial pattern. In this sense, a complementary approach consists in employing an *anisotropic* metasurface in which pumping could induce a transient modulation of static dichroism and birefringence (Della Valle et al., 2017).

Here, following this last strategy, we present an anisotropic AlGaAs metasurface, very efficiently reconfigurable by all-optical means, and showing giant modulations of its dichroic properties on an ultrafast timescale. We combine experiments with theoretical simulations, by performing ultrafast pump-probe spectroscopy and multisteps modelling to rationalize the dynamics of the retrieved transient optical response.

The paper is organized as follows. In section 2 the design of the metasurface is described, and the results of measurements are shown; an account of modelling, as well as the discussion on experimental results, can be found in section 3. Finally, in section 4, some conclusions are drawn about the presented picture, and considerations about ongoing and future work are presented.

2 DESIGN AND EXPERIMENTS

The fabricated sample consists of two replicas of a 4×7 matrix of $70 \mu\text{m} \times 70 \mu\text{m}$ AlGaAs nanowire metasurfaces, each implementing different values of the periodicity P and wires width W . The left panel of figure 1 shows a sketch of one such metasurface, as well as a pictorial depiction of the concept of ultrafast pump-probe spectroscopy. The left inset illustrates the unit-cell vertical cross-section, while the SEM image on the bottom right shows the top-view of the horizontal xy -plane.

We report here measurements and results relative to the metasurface parameters $P = 450 \text{ nm}$, $W =$

180 nm : this specific combination of parameters allows to tune an extended resonance of the unperturbed structure in a spectral range comprised between 750 nm and 800 nm ; such a range is of particular interest due to band-filling, which is the mechanism presiding over the third-order optical nonlinearity in semiconductors at the bandgap edge. Indeed, in such region, the photoinduced permittivity modulation following pump absorption is pronounced and dominated by its real part; thus, nonlinear losses are negligible (Pogna et al., 2021). For the present case of $\text{Al}_{0.2}\text{Ga}_{0.8}\text{As}$, the bandgap sits at around 745 nm .

The right panel of figure 1 shows the measured reflection spectrum of the unperturbed sample for light polarized parallel (TE) or perpendicular (TM) with respect to the nanowires (see inset), impinging at an angle of approximately $\sim 10^\circ$. The diameter of the spot-size (FWHM) of the laser beam employed for probing is approximately $250 \mu\text{m}$, to be compared with the diagonal of the metasurface ($\sim 100 \mu\text{m}$). Thus, the sample is almost uniformly illuminated.

Note that the strong anisotropy of the metasurface directly translates into a markedly dichroic static response. A resonance in the TE polarization is located at around 775 nm , whereas no resonant features are observed upon illumination with TM polarized light. It is also to be remarked that, due to probe spot-size dimensions, the dominant contribution to the spectra comes from light reflected by the substrate. Indeed, we also measured the substrate optical response, which, since an AlOx buffer is present, is configured as the typical Fabry-Perot etalon response. In any case, due to symmetry of quasi-normal incidence, the substrate reflection spectra are almost degenerate in the two different polarizations, and don't show any narrow resonant feature.

With the aim of characterizing the photo-induced modulation of the dichroic properties of the metasurface, we performed ultrafast pump-probe spectroscopy measurements. These consist in illuminating the sample with a high intensity pump pulse and then interrogating it with a second (lower intensity) probe pulse, to record the relative variation of the sample reflection, $\Delta R/R = \frac{R' - R}{R}$, where R' and R are the reflection of the perturbed and unperturbed sample, respectively. This quantity is a function of both the probe wavelength and the time delay between the two pulses.

The experimental apparatus is constructed as follows: a Ti:sapphire laser that emits 100-fs pulses at 800 nm wavelength, with a repetition rate of 1 kHz , pumps a 1 mm Beta-Barium-Borate (BBO) crystal to generate second harmonic pulses, centered at 400 nm . These are directly employed as the optical pump in

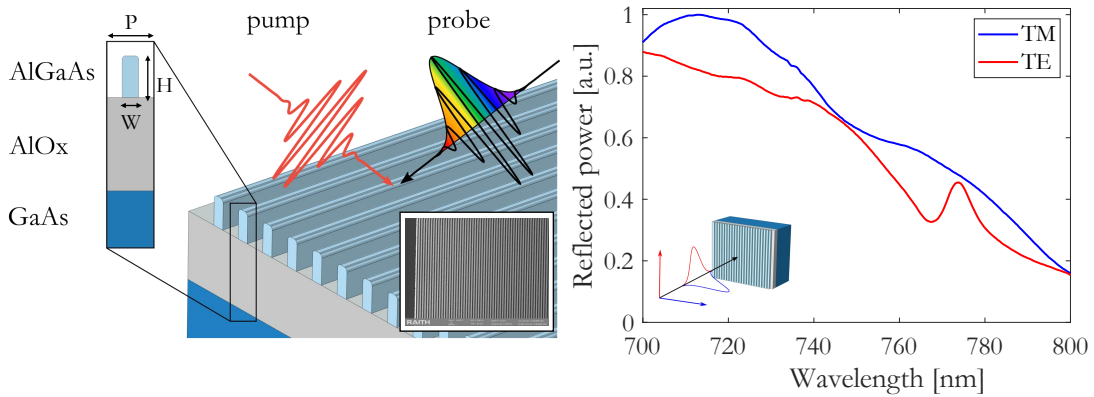


Figure 1: (Left). A depiction of one of the fabricated metasurfaces, together with the illustration of the concept of pump-probe spectroscopy. Left inset shows a vertical cross-section of the unit cell of the structure, with the AlGaAs nanowire on top of a $900 \mu\text{m}$ thick AlOx buffer and GaAs substrate. Bottom right inset is a SEM image showing the corresponding top-view (horizontal plane). (Right). Reflection spectra of the unperturbed sample for light polarized parallel (TE) or perpendicular (TM) with respect to the nanowires orientation, impinging at a small angle ($\theta \simeq 10^\circ$).

the experiment. A non-collinear optical parametric amplifier is used to generate pulses at 1240 nm , to pump in turn a YAG crystal in order to obtain the probe pulse. An optical delay line is inserted along the pump path and the pump is modulated at 500 Hz by a mechanical chopper, so that it is possible to obtain the differential reflection $\Delta R/R$ as a function of the pump-probe delay time.

By properly adding polarizers and waveplates to this configuration, one can record polarization-resolved two-dimensional maps of $\Delta R/R_{\text{TE}}$, $\Delta R/R_{\text{TM}}$. Measurements are shown in figure 2. The transient optical response is strongly dichroic, showing huge modulations (up to $\sim 40\%$) of the reflected power for the TE polarization at a spectral position which corresponds to the neighbourhood of the unperturbed resonant wavelength, whereas in TM the differential signal, though sizable, is much lower. These results are remarkable considering the incident pump fluence of $70 \mu\text{J}/\text{cm}^2$, which can be esteemed a low - moderate level of excitation with respect to the ones reported in literature (Pogna et al., 2021; Mazzanti et al., 2021), and is two orders of magnitude below the damaging threshold of the sample.

The same measurements have been also performed by illuminating the substrate only, i.e. in a region with an AlOx thick film on top of GaAs substrate: in this case, the transient reflectivity response is degenerate in polarization and amounts to less than 2% . Hence, the differential signal, and thus the modulation of dichroism shown in figure 2 is dominated by the AlGaAs metasurface response.

In order to better visualize the complex spectral features of the transient optical response, cross sections of the polarization-resolved 2D maps at fixed time delays of 3 ps , 6 ps and 12 ps can be inspected

in figure 3, with TE/TM polarizations color coded as in previous figures. Concerning TE polarization, one can observe that the peak of the differential reflectance signal is clearly located at $\sim 770 \text{ nm}$, in close correspondence with the static resonance; however, other extremely narrow features are present in the transient map, which cannot be directly related to the shape of the unperturbed spectrum. This could be due to the experimental conditions in which the static reflectivity measurements have been performed: as it has already been remarked upon, the dimension of probe spot-size diameter entails that the reflected power shown in figure 1 is dominated by the substrate contribution. Therefore, narrow spectral features belonging to the metasurface optical response are compensated for or completely covered by substrate reflection; instead, they are revealed in the transient measurements, where high reflectivity of the background is almost fully rejected.

It is to be noted that the effect is in practice extinguished within 12 ps from pump arrival.

3 MODELLING AND DISCUSSION

In order to rationalize the efficient reconfiguration of the metasurface following photoexcitation, we decided to adopt a simplified version of a multistep model which describes the physical processes taking place following photoexcitation (Mazzanti et al., 2021). We will now briefly summarize such mechanisms and how they are taken into account in the model, as schematically depicted in figure 4.

AlGaAs is a direct bandgap semiconductor with

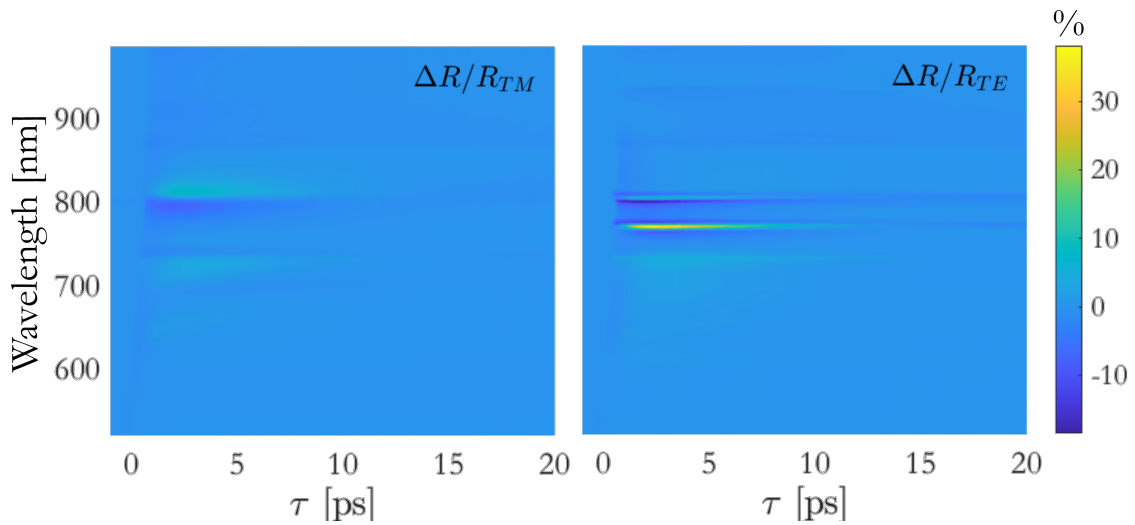


Figure 2: Measured 2D maps of differential reflection, retrieved as a function of probe wavelength and pump-probe time delay, for the TM (left) and TE polarization (right).

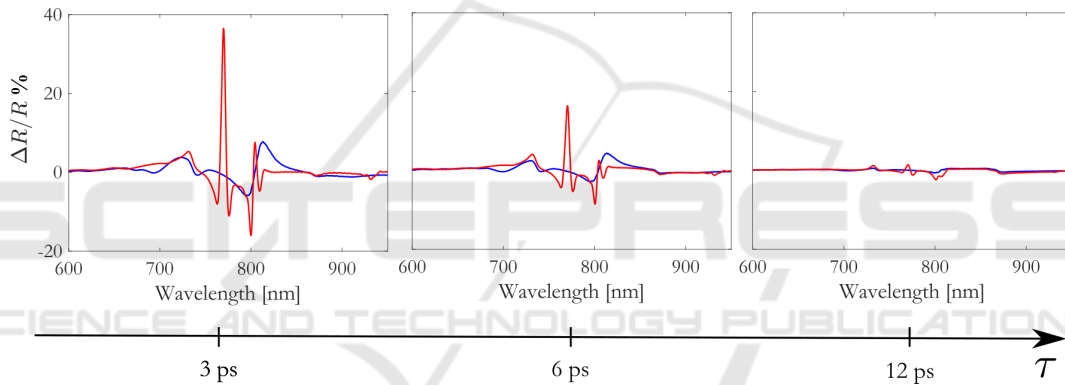


Figure 3: Cross-sections of the 2D maps of figure 2 at a time delay of 3 ps (left), 6 ps (centre) and 12 ps (right). Red (blue) curve corresponds to TE (TM) polarization.

gap energy $E_{\text{gap}} \simeq 1.65$ eV. Absorption of the pump pulse, which is centered at $\lambda = 400$ nm with an energy of 3.2 eV, generates a population of electron-hole pairs in the conduction and valence band respectively, via interband transitions.

The photoexcited population of electron-holes then recombines through different channels: trap-assisted nonradiative recombination, bimolecular and Auger processes, the first one being the dominating due to the large surface-to-volume ratio of nanostructures (Shcherbakov et al., 2017). Nonradiative recombination entails the emissions of phonons, and thus a slow increase of the lattice temperature in the wires.

The aforementioned degrees of freedom of the photoexcited system – namely, the density of e-h pairs and the lattice temperature – and their evolution in time can be described with the simple rate equation system depicted in figure 4. This is the so-called Two

Temperature Model (TTM).

Electron-holes pairs can be conceived as a plasma, contributing to an ultrafast change of AlGaAs permittivity through two distinct mechanisms. One is the typical Drude process, for intraband transitions, entailing a modification $\Delta\epsilon_{\text{Drude}}$. The second effect is the so called band-filling (hence the permittivity variation $\Delta\epsilon_{\text{BF}}$), which accounts for a saturation of the absorption channels: since the bottom of the conduction band has been filled with electrons promoted following photoexcitation, Pauli exclusion principle forbids interband transitions upon arrival of the probe beam. This entails a modification of the imaginary part of the material permittivity for probe wavelengths with energy above the bandgap; hence, modulation of the real part of permittivity is determined through Kramers-Krönig relations. Crucially, the probe beam having an energy below the bandgap (i.e. in the present case

at wavelengths longer than ~ 745 nm) experiences a permittivity modulation due to band filling which is purely real. Therefore, in such spectral regions near the bandgap, where band filling dominates, losses are minimized. Finally, another contribution to permittivity modulation comes from the lattice heating through thermo-optics effect, $\Delta\epsilon_{\text{thermo}}$. We refer the reader to (Mazzanti et al., 2021) for the exact expression of each contribution to the transient permittivity change as a function of the electron-hole couple density and lattice temperature.

Therefore, by resolving the TTM and directly substituting the solution into the described semiclassical formulas, it is possible to model the ultrafast permittivity variation as a function of time delay and probe wavelength. Transient optical response of the sample can then be retrieved by performing full vectorial electromagnetic simulations.

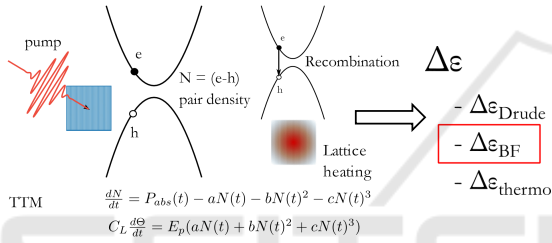


Figure 4: Schematics of physical processes taking place following photoexcitation, together with the steps of the model: TTM to describe electron-hole pairs density and lattice temperature as they evolve in time, semiclassical formulas to compute permittivity variations due to Drude, band filling and thermo-optics mechanisms.

This approach, though accurate, is also computationally demanding. We decided to start with a simple estimate of the permittivity variation at the time delay corresponding to the signal peak (3 ps) with respect to the spectral region near the bandgap. The selected timescale allows us to neglect the thermo-optics permittivity variation, since the lattice heating is a slower process. Instead, the most relevant mechanism is represented by band filling, which also dominates over Drude effect (Mazzanti et al., 2021). As a further simplification, we also decided to set a fixed (real valued) permittivity change for all the interesting wavelength range (700–800 nm), in order to highlight the key features of the considered phenomenon. Therefore, we solved the TTM using the same material parameters for AlGaAs as in (Mazzanti et al., 2021) and considering a pump fluence of $35 \mu\text{J}/\text{cm}^2$ – half the experimental value – to correct the model’s permittivity variation overestimation for a factor of two, as explained in the same paper. Then, we chose the computed value at $\lambda = 745$ nm, $t = 3$ ps as the uniform

permittivity variation, $\Delta\epsilon = -0.08$.

This is a rather coarse approximation, disregarding both the imaginary part and spectral dependence of $\Delta\epsilon$. However, the imaginary part of permittivity change is nonzero only for wavelengths shorter than 745 nm, since band-filling effect dominates; moreover, our model reveals that in this same spectral region the real permittivity variation is more dispersed, whereas it is flatter in the region between 745 nm and 800 nm. Thus, we should expect an acceptable qualitative accuracy in the interesting spectral range where most important modifications of the optical response occur.

We then performed full-vectorial electromagnetic simulations employing commercial software COMSOL Multiphysics 6, to compute both the static optical response of the metasurface ($\Delta\epsilon = 0$) and the perturbed one ($\Delta\epsilon = -0.08$). We set the following parameters for the structure geometry: periodicity $P = 435$ nm, wires width $W = 185$ nm and wires height $H = 415$ nm (nominal fabrication parameter was $H = 400$ nm). These values are optimized to fit the static optical response to the experimental spectra, in order to take into account fabrication defects and boundary effects which cannot be included in simulations with periodic boundary conditions.

Results are shown in right panel of figure 5. On the left, for comparison, the experimental differential reflection curves at 3 ps are plotted with the same vertical axis. For TM polarization (blue curves) the agreement is remarkably good, with a slight quantitative overestimation of the transient effects at short wavelengths and between 780–800 nm. This can be ascribed to the choice of fixing the permittivity to the value corresponding to $\lambda = 745$ nm and neglecting losses in the range 700–745 nm. Something similar happens also for TE polarization; notice however the accurate estimation of the peak differential reflectivity at 769 nm (760 nm in the simulation). Difference in narrow features in the range 760–780 nm (specifically, the pronounced dip at 765 nm in the simulation) has instead to be attributed to an imperfect fit of the geometrical parameters, which was performed to accurately mimic the experimental sample response.

Nevertheless, notwithstanding the approximations, our model is capable of highlighting the origin of such efficient modulation of the sample dichroic response, attributing it to the combination of two factors: (a) the dominant contribution of band filling to permittivity modulation, which is purely real in the spectral range of interest, thus allowing to minimize losses, and (b) the presence of sharp resonances of the metasurface in this precise spectral region near the bandgap.

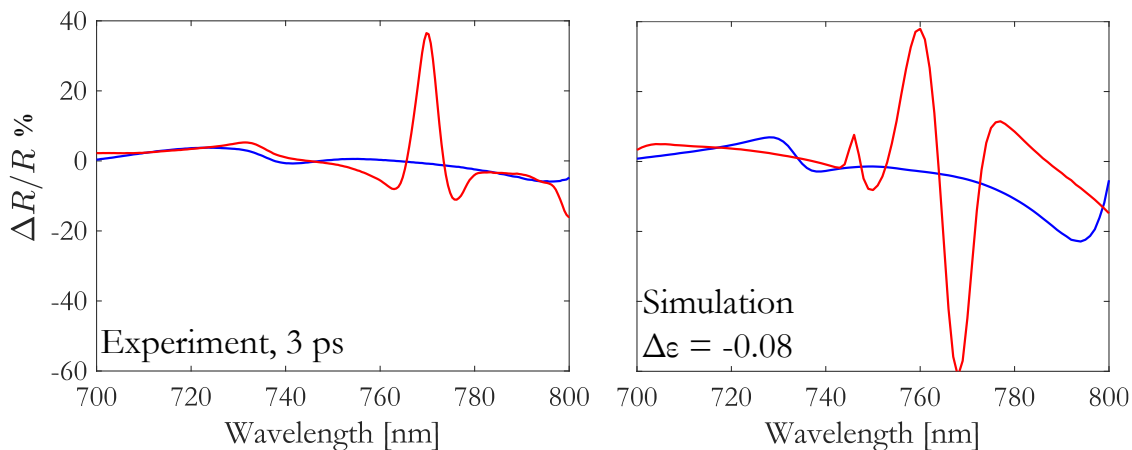


Figure 5: (Left). Experimental differential reflection at 3 ps. Red (blue) curve corresponds to a TE (TM) polarized probe. (Right). Simulated differential reflection obtained for a uniform permittivity modulation $\Delta\epsilon = -0.08$, corresponding to the value obtained by our model at $t = 3$ ps, $\lambda = 745$ nm. Color coding corresponds to the one of left panel. Vertical axis is shared among the two panels.

4 CONCLUSIONS

We have presented an anisotropic metasurface based on AlGaAs nanowires on top of a composite AlO_x-GaAs substrate, to be used as a platform for dichroism modulation through all-optical schemes, to the aim of obtaining ultrafast control of light polarization. We experimentally demonstrated very high efficiency in reshaping the optical response (with a differential reflection peak of almost 40%) in the 700 – 800 nm spectral range, with a moderate excitation fluence of $70 \mu\text{J}/\text{cm}^2$.

Our preliminary, simplified version of the multi-physics modelling laid out in section 3 is capable of capturing the key physical phenomena taking place after photoexcitation and regulating the transient optical response: specifically, high modulation is obtained by exploiting a sharp resonance of the structure in the spectral region near to the bandgap, and the measured effect is to be attributed to band-filling as the dominant mechanism presiding over the ultrafast permittivity change. Since this contribution is purely real for the interesting range of operation, losses are extremely reduced. From the designer perspective, this conclusion can suggest a suitable direction to follow, with the goal of tailoring the static optical response of devices by tuning narrow spectral features near the bandgap region of the constituent metasurface semiconductor.

As for modelling, further steps (and work in progress) include the employment of the full model to elucidate the temporal dynamics of the transient optical signal. In addition, an interesting future perspective is represented by the possibility of studying the

reconfiguration of the birefringent properties of such metasurfaces, possibly tailoring them to the ambitious goal of implementing ultrafast waveplate functionalities.

ACKNOWLEDGEMENTS

This publication is part of the METAFast project that received funding from the European Union Horizon 2020 Research and Innovation program under grant agreement no. 899673. This work reflects only authors' view and the European Commission is not responsible for any use that may be made of the information it contains.

REFERENCES

- Della Valle, G., Hopkins, B., Ganzer, L., Stoll, T., Rahmani, M., Longhi, S., Kivshar, Y. S., Angelis, C. D., Neshev, D. N., and Cerullo, G. (2017). Nonlinear anisotropic dielectric metasurfaces for ultrafast nanophotonics. *ACS Photonics*, 4(9):2129–2136.
- Flamini, F., Spagnolo, N., and Sciarrino, F. (2018). Photonic quantum information processing: a review. *Reports on Progress in Physics*, 82(1):016001.
- Fleischer, S., Zhou, Y., Field, R. W., and Nelson, K. A. (2011). Molecular orientation and alignment by intense single-cycle THz pulses. *Physical Review Letters*, 107(16).
- Först, M., Manzoni, C., Kaiser, S., Tomioka, Y., Tokura, Y., Merlin, R., and Cavalleri, A. (2011). Nonlinear phononics as an ultrafast route to lattice control. *Nature Physics*, 7(11):854–856.

- Mazzanti, A., Pogna, E. A. A., Ghirardini, L., Celebrano, M., Schirato, A., Marino, G., Lemaître, A., Finazzi, M., Angelis, C. D., Leo, G., Cerullo, G., and Valle, G. D. (2021). All-optical modulation with dielectric nanoantennas: Multiresonant control and ultrafast spatial inhomogeneities. *Small Science*, 1(7):2000079.
- Nicholls, L. H., Rodríguez-Fortuño, F. J., Nasir, M. E., Córdova-Castro, R. M., Olivier, N., Wurtz, G. A., and Zayats, A. V. (2017). Ultrafast synthesis and switching of light polarization in nonlinear anisotropic metamaterials. *Nature Photonics*, 11(10):628–633.
- Pogna, E. A. A., Celebrano, M., Mazzanti, A., Ghirardini, L., Carletti, L., Marino, G., Schirato, A., Viola, D., Laporta, P., Angelis, C. D., Leo, G., Cerullo, G., Finazzi, M., and Valle, G. D. (2021). Ultrafast, all optically reconfigurable, nonlinear nanoantenna. *ACS Nano*, 15(7):11150–11157.
- Schirato, A., Maiuri, M., Toma, A., Fugattini, S., Zaccaria, R. P., Laporta, P., Nordlander, P., Cerullo, G., Alabastri, A., and Valle, G. D. (2020). Transient optical symmetry breaking for ultrafast broadband dichroism in plasmonic metasurfaces. *Nature Photonics*, 14(12):723–727.
- Shcherbakov, M. R., Liu, S., Zubyuk, V. V., Vaskin, A., Vabishchevich, P. P., Keeler, G., Pertsch, T., Dolgova, T. V., Staude, I., Brener, I., and Fedyanin, A. A. (2017). Ultrafast all-optical tuning of direct-gap semiconductor metasurfaces. *Nature Communications*, 8(1).
- Stanciu, C. D., Hansteen, F., Kimel, A. V., Kirilyuk, A., Tsukamoto, A., Itoh, A., and Rasing, T. (2007). All-optical magnetic recording with circularly polarized light. *Physical Review Letters*, 99(4).
- Wang, K., Li, M., Hsiao, H.-H., Zhang, F., Seidel, M., Liu, A.-Y., Chen, J., Devaux, E., Genet, C., and Ebbesen, T. (2021). High contrast, femtosecond light polarization manipulation in epsilon-near-zero material coupled to a plasmonic nanoantenna array. *ACS Photonics*, 8(9):2791–2799.
- Yang, Y., Kelley, K., Sachet, E., Campione, S., Luk, T. S., Maria, J.-P., Sinclair, M. B., and Brener, I. (2017). Femtosecond optical polarization switching using a cadmium oxide-based perfect absorber. *Nature Photonics*, 11(6):390–395.